Spin-orbit couplings within spin-conserving and spin-flipping time-dependent density functional theory: Implementation and benchmark calculations

Saikiran Kotaru^a, Pavel Pokhilko^{a,b}, and Anna I. Krylov^{a,*}

- ^a Department of Chemistry, University of Southern California, Los Angeles, California 90089-0482, USA
- b Present address: Department of Chemistry, University of Michigan, Ann Arbor, Michigan 48109, USA
 - * Corresponding author: krylov@usc.edu

We present a new implementation for computing spin-orbit couplings (SOCs) within time-dependent density-functional theory (TD-DFT) framework in the standard spin-conserving formulation as well in the spin-flip variant (SF-TD-DFT). This approach employs the Breit-Pauli Hamiltonian and Wigner-Eckart's theorem applied to the reduced one-particle transition density matrices, together with the spin-orbit mean-field (SOMF) treatment of the two-electron contributions. We use state-interaction procedure and compute the SOC matrix elements using zero-order non-relativistic states. Benchmark calculations using several closed-shell organic molecules, diradicals, and a single-molecule magnet (SMM) illustrate the efficiency of the SOC protocol. The results for organic molecules (described by standard TD-DFT) show that SOCs are insensitive to the choice of the functional or basis sets, as long as the states of the same characters are compared. In contrast, the SF-TD-DFT results for small diradicals (CH₂, NH $_2^+$, SiH₂, and PH $_2^+$) show strong functional dependence. The spin-reversal energy barrier in a Fe(III) SMM computed using noncollinear SF-TD-DFT (PBE0, ωPBEh/cc-pVDZ) agrees well with the experimental estimate.

I. INTRODUCTION

Spin-orbit coupling (SOC) is a relativistic effect arising from the interaction of the orbital angular momentum of an electron with its intrinsic spin angular momentum. SOC plays

a crucial role in various chemical phenomena. For example, SOC determines magnetic properties of single-molecule magnets (SMMs) and rates of spin-forbidden processes^{1–6} such as phosphorescence, intersystem crossing, and, more generally, nonadiabatic dynamics of molecules and materials.^{7–11} In SMMs, it leads to magnetic anisotropy, thereby affecting the spin-reversal energy barrier and magnetic relaxation. Although SOC is much larger in heavy atoms, it also plays a role in systems composed of light atoms, such as organic molecules.¹²

An accurate quantum-mechanical treatment of SOC is required in many applications.^{13–18} SOC is commonly computed using the state interaction scheme—often called a perturbative approach—in which a small number of zero-order non-relativistic states are used to compute the matrix elements of the Breit-Pauli Hamiltonian, followed by the diagonalization of the resulting matrix to yield the spin–orbit coupled states and energies.^{19,20} The Breit-Pauli Hamiltonian contains one- and two-electron parts, with the latter being about 50 % of the total contribution in light molecules. The costs of computing the two-electron contribution can be be significantly reduced using an effective one-electron spin–orbit mean-field (SOMF) approximation.^{21–23}

Various implementations employing full and approximate Breit-Pauli SOC operators have been reported for density-functional theory (DFT),^{24–29} density-functional theory/multireference configuration interaction (DFT/MRCI),^{30,31} coupled-cluster (CC),³² equation-of-motion CC (EOM-CC),^{33–36} multireference CC (MRCC),³⁷ complete active-space self-consistent field (CASSCF),^{19,38,39} restricted active space self-consistent field (RASSCF),⁴⁰ restricted active space configuration interaction (RASCI),⁴¹ MRCI,⁴² and density-matrix renormalization group (DMRG)^{43,44} methods.

In contrast to matrix elements describing non-relativistic transition properties—such as nonadiabatic couplings or transition dipole moments—SOCs are tensorial quantities requiring calculations between all the components of the interacting multiplets. Wigner-Eckart's theorem^{45–47} allows one to circumvent the explicit calculation of all multiplet components by providing a recipe for generating the full set of the SOC matrix elements from just one spin projection, for example, the $M_s = 0$ component. Using this strategy, Pokhilko *et al.* developed a framework for computing SOCs by the application of Wigner-Eckart's theorem to the reduced one-particle density matrices.³⁶ The efficiency of this protocol was illustrated by application to the EOM-CC wave-functions. Formulated in spin-orbital representation, this approach is ansatz-agnostic and can be applied to any electronic structure method that can

provide transition density matrices. Following this work, SOCs for frozen-core core-valence separated EOM-CCSD (fc-CVS-EOM-CCSD),⁴⁸ RASCI, and RAS-spin-flip (RAS-SF)^{41,49} wave functions were implemented.

Here, we extend this algorithm³⁶ to compute SOCs using time-dependent DFT (TD-DFT)⁵⁰ in its standard spin-conserving and spin-flipping (SF-TD-DFT)^{51–55} variants within the Tamm-Dancoff approximation (TDA).⁵⁶ Owing to its favorable computational scaling, TD-DFT is often employed to calculate excited states in extended systems. Implementations of SOCs between the TD-DFT states are available in program packages such as MolSOC²⁵ and PySOC²⁸, however, the SOCs for SF-TD-DFT have not yet been reported. The SF approach extends Kohn-Sham TD-DFT to treat certain types of strong correlation, such as bond-breaking, conical intersections, and systems with two or more unpaired electrons.^{55,57–59}

This work describes the implementation of SOCs using TD-DFT and SF-TD-DFT within the Q-Chem electronic structure package^{60,61} and presents benchmark results for molecules featuring different types of electronic structure: e.g., closed-shell organic molecules, diradicals, and a molecular magnet. We compare the results obtained with different DFT and wave-function-based methods and assess the effect of specific density functionals and basis sets on the SOC. The paper is organized as follows. Section II presents the theory of TD-DFT/TDA and SF-TD-DFT/TDA, and the key equations for the calculation of the Breit-Pauli SOC matrix elements using Wigner-Eckart's theorem. The computational details are given in Section III. Sections IV A and IV B provide the benchmark results obtained using TD-DFT and SF-TD-DFT, respectively. Our concluding remarks are given in Section V.

II. THEORY

A. TD-DFT/TDA and SF-TD-DFT/TDA

Within TDA, TD-DFT treatment involves solving the following Hermitian eigenvalue equation:

$$AX = X\Omega, \tag{1}$$

with

$$A = \delta_{ab}\delta_{ij} \left(\epsilon_a - \epsilon_i\right) + \left(ia|jb\right) + \left(ia|f_{xc}|jb\right), \tag{2}$$

where indexes i, j denote the occupied orbitals, a, b denote the virtual orbitals, ϵ_a and ϵ_i are the orbital energies of the virtual and occupied Kohn-Sham orbitals, respectively, f_{xc} is the adiabatic exchange-correlation kernel, Ω is a diagonal matrix with excitation energies on the diagonal, X contains the eigen-vectors of A, and the two-electron integrals are given in Mulliken's notation. TD-DFT/TDA yields excitation energies very close to the corresponding (linear response) TD-DFT excitation energies for closed- and open-shell molecules. ⁵⁶ In SF-TD-DFT, a high-spin reference is used to describe target multi-configurational lower-spin states by spin-flipping excitations as:

$$\Psi_{M_s=S-1}^{S,S-1} = \hat{R}_{M_s=-1} \Psi_{M_s=S}^S, \tag{3}$$

where the spin-flip operator $\hat{R}_{M_s=-1}$ generates singly excited determinants in which the spin of one electron is flipped with respect to the high-spin reference.⁵⁵

In the standard collinear formulation, the target spin-flipped determinants can only be coupled by the Hartree-Fock exchange; hence, in the original SF-TD-DFT method functionals with high fractions of the exact exchange—such as B5050LYP—were employed⁵¹. This limitation was overcome by using non-collinear formulation.^{52–54} Previous benchmark studies for organic diradicals⁵⁴, binuclear Cu(II)⁶² and Fe(III)⁵⁸ SMMs illustrated robust performance of the non-collinear SF-TD-DFT, especially when combined with the functionals from the PBE family. Here, we use the best performing functionals to assess the performance of the SF-TD-DFT for computing SOCs in selected diradicals and in a Fe(III) SMM.

B. Spin-orbit Hamiltonian

Originally derived by Pauli, 63,64 the Breit-Pauli Hamiltonian describes the relativistic effects. In particular, it can be used to evaluate spin-orbit matrix elements between non-relativistic electronic states. In atomic units, the spin-orbit part of the Breit-Pauli Hamiltonian has the following form:

$$H_{\rm BP}^{\rm SO} = \frac{1}{2c^2} \left[\sum_{i} \sum_{K} \frac{Z_k(\mathbf{r}_i - \mathbf{R}_K) \times \mathbf{p}_i}{|\mathbf{r}_i - \mathbf{R}_K|^3} \cdot \mathbf{s}(i) - \sum_{i \neq j} \frac{(\mathbf{r}_i - \mathbf{r}_j) \times \mathbf{p}_i}{|\mathbf{r}_i - \mathbf{r}_j|^3} \cdot (\mathbf{s}(i) + 2\mathbf{s}(j)) \right]$$
(4)

where c is the speed of light, \mathbf{r}_i and \mathbf{p}_i denote the coordinate and momentum operators of the *i*th electron respectively, $\mathbf{s}(i)$ is the spin operator, and \mathbf{R}_K and Z_K are the coordinates and the charge of the *K*th nucleus. The first term, the one-electron part of the Breit-Pauli Hamiltonian, is proportional to the nuclear charge and, therefore, dominates in heavy elements. The second term, the two-electron part of the Hamiltonian, describes spin-same-orbit and spin-other-orbit interactions; it is significant in molecules composed of light atoms, such as typical organic molecules.²⁰ Full calculations of SOC involves computation of one-and two-particle transition density matrices and contracting them with appropriate spin-orbit integrals.³⁵ Fortunately, the cost of the evaluation of the two-electron contribution can be significantly reduced by invoking spin-orbit mean-field (SOMF) approximation.²¹ The SOMF approximation amounts to considering only the contributions from the separable part of the two-particle density matrix,³⁵ which captures most of the effect leading to insignificant errors.

The symmetry of the one-electron term in Eq. (4) is such that one can write down the second-quantized form of it using triplet excitation operators. Here, we use the irreducible spherical tensor operators to represent the SOMF Hamiltonian. The triplet excitation operators are given in the second quantization as:

$$T_{pq}^{1,1} = -a_{p\alpha}^{\dagger} a_{q\beta}, \tag{5}$$

$$T_{pq}^{1,0} = \frac{1}{\sqrt{2}} \left(a_{p\alpha}^{\dagger} a_{q\alpha} - a_{p\beta}^{\dagger} a_{q\beta} \right), \tag{6}$$

$$T_{pq}^{1,-1} = a_{p\beta}^{\dagger} a_{q\alpha}, \tag{7}$$

where the $T^{1,\pm 1}$ are spin-flipping (change the spin-projection) and $T^{1,0}$ conserves the spin projection. Using these operators, the SOMF Hamiltonian can be written as:

$$H^{\text{SOMF}} = \frac{1}{2} \sum_{pq} \left[h_{L_{+},pq}^{\text{SOMF}} T_{pq}^{1,-1} + h_{z,pq}^{\text{SOMF}} T_{pq}^{1,0} + h_{L_{-},pq}^{\text{SOMF}} T_{pq}^{1,1} \right], \tag{8}$$

where $h_{L_+,L_-}^{\rm SOMF}$ are constructed using the sum of one-electron and mean-field contributions:

$$h_{L_{+}}^{\text{SOMF}} = h_{x}^{\text{SOMF}} + ih_{y}^{\text{SOMF}}, \tag{9}$$

$$h_{L_{-}}^{\text{SOMF}} = h_{x}^{\text{SOMF}} - ih_{y}^{\text{SOMF}}.$$
 (10)

In the above expression, the two-electron spin—orbit integrals are contracted with the density matrix of the reference state (hence, mean-field).

Through the application of Wigner–Eckart's theorem to the triplet excitation operators, Eq. (8) can be implemented as:

$$\langle I'S'M'|T_{pq}^{1,M}|I''S''M''\rangle = \langle S''M'';1M|S'M'\rangle \langle I'S'||T_{pq}^{1,\cdot}||I''S''\rangle,$$
 (11)

where $|I'S'M'\rangle$ denotes the I'th electronic state with spin S' and spin-projection M' respectively, $\langle S''M''; 1M|S'M'\rangle$ is a Clebsh–Gordan coefficient, and $\langle I'S'||T_{pq}^{1,\cdot}||I''S''\rangle$ is a spinless triplet transition density matrix (denoted as u_{pq} below). u_{pq} can be obtained³⁶ from the one-particle transition density matrix between the states with the same spin projection as:

$$u_{pq} \equiv \langle I'S' || \hat{T}_{pq}^{1,\cdot} || I''S'' \rangle = \frac{1}{\sqrt{2}} \left(\gamma_{pq,\alpha\alpha}^{\Delta M_s = 0} - \gamma_{pq,\beta\beta}^{\Delta M_s = 0} \right) / \langle S''M'; 10 | S'M' \rangle, \tag{12}$$

where the transition density matrix γ_{pq} is defined as:

$$\gamma_{pq} = \langle I'S'M'|a_p^{\dagger}a_q|I''S''M'\rangle. \tag{13}$$

The SOC matrix elements between any two spin-states can then be obtained as:

$$\langle I'S'M'|H^{\text{SOMF}}|I''S''M''\rangle = \frac{1}{2} \sum_{pq} \left[h_{L_+,pq}^{\text{SOMF}} \langle S''M''; 1 - 1|S'M'\rangle + \sqrt{2} h_{z,pq}^{\text{SOMF}} \langle S''M''; 10|S'M'\rangle - h_{L_-,pq}^{\text{SOMF}} \langle S''M''; 11|S'M'\rangle \right] u_{pq}.$$

$$(14)$$

We use the u_{pq} matrix between spin-multiplets $|S'M'\rangle$ and $|S''M'\rangle$ to compute the entire set of the SOC matrix elements for all pairs of the interacting spin-states: $-S' \leq M' \leq S'$ and $-S'' \leq M'' \leq S''$. Further details of the theory can be found in Ref. 36.

The key quantity involved in the calculation of inter-system crossing rates and oscillator strengths is the SOC constant (SOCC). While couplings between different multiplet components are dependent on spatial orientation, the SOCC is rotationally invariant and can be computed by taking the sum over all projections as:

$$SOCC = \sqrt{\sum_{M',M''} |\langle S'M'|H^{SO}|S''M''\rangle|^2},$$
(15)

In this work, we use the SOCC values to benchmark with those previously available in the literature.

III. COMPUTATIONAL DETAILS

Fig. 1 shows the structures of the molecules used for benchmarking in this work; below, we refer to the molecules by the letters shown in the figure.

Molecules **a-g** are representative closed-shell organic molecules. Their excited states and SOCs are calculated using standard TD-DFT/TDA. Ground-state optimized geometries of formaldehyde and acetone (molecules **a** and **b**, at ω B97XD/TZVP) and psoralens (molecules **e-g**, at PBE0/TZVP) are taken from Ref. 28, and biacetyl (BIA) and (2Z)-2-buten-2-ol (BOL) (molecules **c** and **d**, at B3LYP/cc-pVDZ) are taken from Ref. 41.

Molecules \mathbf{h} - \mathbf{q} feature electronic degeneracies of the frontier orbitals and, therefore, cannot be described by standard Kohn-Sham TD-DFT. To compute relevant spin-states in this set, we use the non-collinear formulation of SF-TD-DFT/TDA. For diradicals \mathbf{h} - \mathbf{k} we use equilibrium triplet-state geometries (${}^{3}\mathrm{B}_{2}$), following the previous studies. Experimental structures are used for molecules \mathbf{l} - \mathbf{p} , taken from Ref. 32, and the structure of the trigonal bipyramidal Fe(III) SMM (molecule \mathbf{q}) is taken from Ref. 69. High-spin triplet reference was used to compute target triplet and singlet spin-flip states in molecules \mathbf{h} - \mathbf{p} . To access the quartet ground state in molecule \mathbf{q} , a high-spin hextet reference was used.

We tested functional dependencies of the SOC for formaldehyde and acetone by considering B3LYP,⁷⁰ PBE0,⁷¹ ω PBEh,⁷² ω B97X-D,⁷³ and ω B97M-V⁷⁴, and basis set dependencies by considering cc-pVTZ and aug-cc-pVTZ. For organic molecules **c**, **d** and **e-g** we used B3LYP with the cc-pVTZ and cc-pVDZ bases, respectively. Similarly, for diradicals **h-k** we tested the effect of the functional choice on SOCs using the cc-pVTZ basis. We used PBE0 and ω PBEh functionals with the cc-pCVTZ and cc-pVDZ basis sets for molecules **l-p** and **q**, respectively. Cartesian coordinates for all molecules are given in the supplementary information (SI).

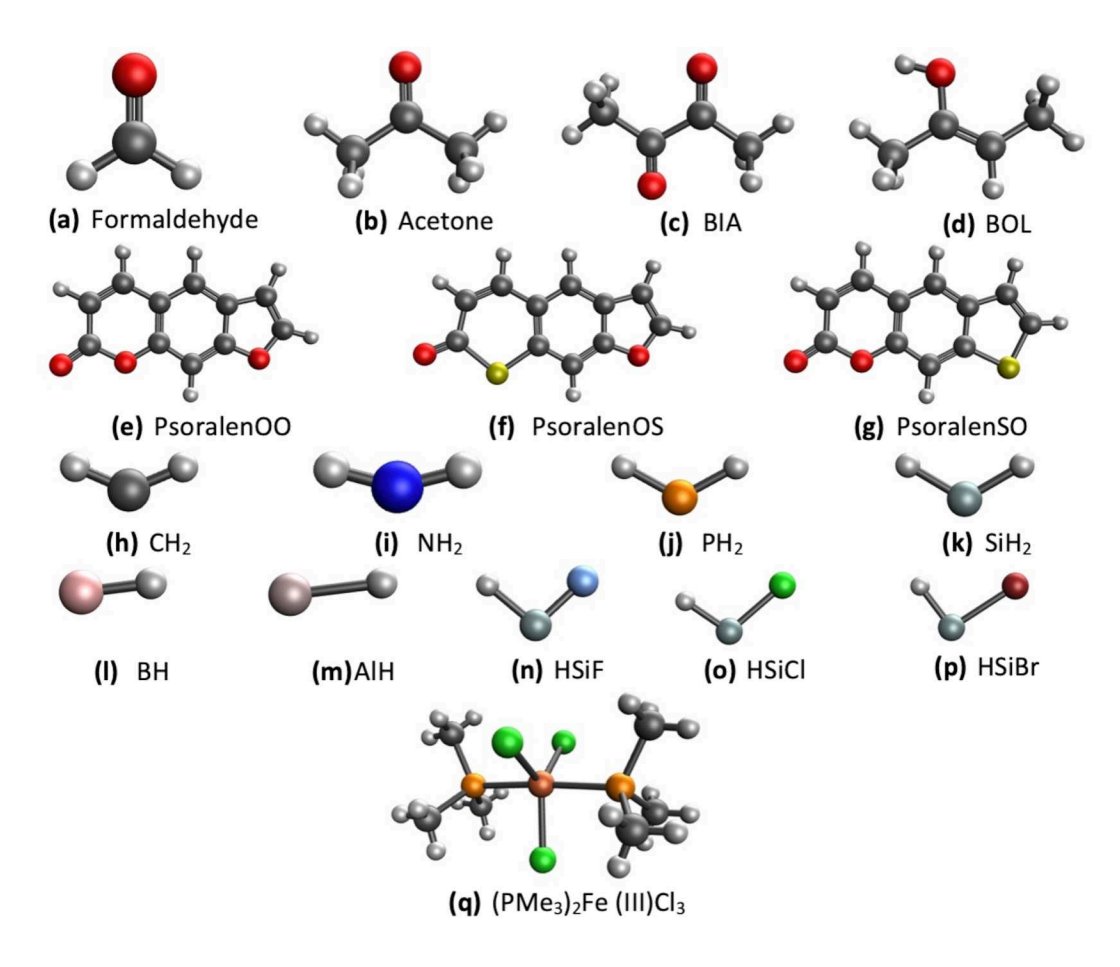


FIG. 1: Molecules studied in this work. BIA and BOL denote biacetyl and (2Z)-2-buten-2-ol, respectively.

To assign the state characters, we used natural transition orbitals (NTOs), the respective leading singular values (σ), and NTO participation ratio (PR_{NTO}),^{75–77} which defines the number of NTO pairs necessary to describe the excitation. σ^2 gives the weights of the electronic transitions between the NTOs. Using dominant excitations, NTOs and descriptors, we carefully compare the states obtained in this work with those reported in previous studies in order to make meaningful comparisons of the respective SOCs.

We use the following acronyms for SOCs taken from previous studies: '1e-eff' for SOCs obtained using effective charges with the one-electron part of the Breit-Pauli Hamiltonian, '1e' for SOCs computed with only the one-electron part of the Breit-Pauli Hamiltonian, 'SOMF' for SOCs obtained using spin-orbit mean-field approximation, 'full BP' for SOCs obtained using the full Breit-Pauli Hamiltonian.

All calculations were performed using the Q-Chem software^{60,61} in which the presented

approach was implemented and released in version 6.0.

IV. RESULTS AND DISCUSSION

A. Spin-orbit couplings in selected organic molecules

1. Formaldehyde and acetone

We first consider carbonyl compounds formaldehyde and acetone and investigate the effect of the functional and basis sets on the SOC. We use hybrid functionals (B3LYP, PBE0) and range-separated hybrid functionals (LRC- ω PBEh, ω B97X-D, and ω B97M-V) and the cc-pVTZ and aug-cc-pVTZ basis sets. The results for formaldehyde and acetone have been reported previously by Gao et al. (employing the one-electron Breit-Pauli operator with an effective charge approximation) using TD-DFT and TD-DFTB, ²⁸ by de Carvalho et al. (using one-electron Breit-Pauli operator) using TD-DFT, ²⁷ by Dinkelbach et al. (using SOMF) using TD-DFT, ²⁹ and Liu et al. ('1e-eff') using semiempirical orthogonalization-corrected methods (OMx) combined with configuration interaction with single excitations (CIS) OMx/CIS and LR-TD-DFT. ¹¹ Below, we compare the spin-orbit coupling constants from PySOC by Gao et al. with our TD-DFT/TDA calculations. ²⁸ We also perform calculations using the highly accurate EOM-EE-CCSD method, which we use as a reference for this study.

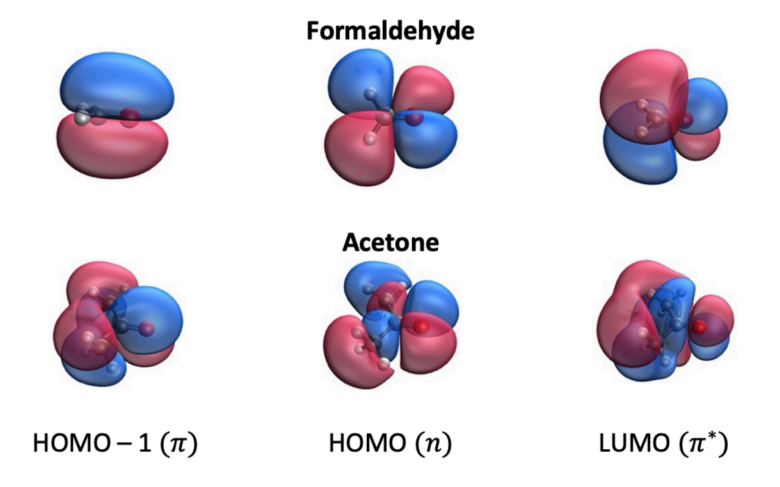


FIG. 2: Canonical Kohn-Sham molecular orbitals $(\pi, n, \text{ and } \pi^*)$ of formaldehyde and acetone (the shapes of the NTOs from the excited-state calculations are very similar); B3LYP/cc-pVTZ.

Fig. 2 shows the relevant molecular orbitals involved in the S_1 , T_1 , and T_2 excited states. With the cc-pVTZ basis, irrespective of the choice of the functional, the lowest singlet state, S_1 is of $n\pi^*$ character, and triplet states T_1 and T_2 are of $n\pi^*$ and π^* character, respectively. Tables S1 and S2 present the vertical excitation energies calculated using different functionals with cc-pVTZ and aug-cc-pVTZ as well as the EOM-EE-CCSD values. The excitation energies computed with different functionals are within 0.3 eV, with S_1 lying between T_1 and T_2 states. The choice of the basis, cc-pVTZ versus aug-cc-pVTZ, has a small effect on the excitation energies with a difference of less than 0.06 eV.

Tables I and II show the SOMF SOCCs computed between the ground state, excited singlet and triplet states in formaldehyde and acetone using the cc-pVTZ and aug-cc-pVTZ bases with different functionals. The one-electron SOCC computed with cc-pVTZ is reported in Table S6. In agreement with El-Sayed's rules, 78,79 the SOC is large for transitions involving a change of the orbital type, i.e., SOC is large between the $^1n\pi^*/^3\pi\pi^*$ states and negligible between $^1n\pi^*/^3n\pi^*$ states. Both one-electron and SOMF SOCCs are insensitive to the choice of functionals and basis sets, with a variation of less than 2 cm⁻¹. While the SOCC between the ground state and $^3n\pi^*$ computed using different functionals matches perfectly with the EOM-EE-CCSD value, the SOCC between the $^1n\pi^*$ and $^3\pi\pi^*$ states differ by about 12 cm⁻¹ and 8 cm⁻¹, with the EOM-CCSD for the one-electron and SOMF parts. A comparison with 1e-eff values (obtained using effective charges by Gao et al. 28) shows a close match with SOMF SOCCs in this study, however, the full Breit-Pauli SOCC (full BP-B3LYP/DALTON) differs by about 10 cm⁻¹ for the $^1n\pi^*/^3\pi\pi^*$ transition.

TABLE I: SOMF SOCCs in formal dehyde and acetone computed with TD-DFT/TDA (B3LYP, PBE0, ω PBEh, ω B97XD, and ω B97M-V) and EOM-EE-CCSD using cc-pVTZ compared with values from Ref. 28.

Transition	B3LYP	PBE0	$\omega PBEh$	$\omega B97$	$\omega B97$	EOM-EE-	B3LYP/	B3LYP/
				X-D	M-V	CCSD	$PySOC^a$	$Dalton^b$
			For	malde	ehyde			
$\mathrm{GS}/^3n\pi^*$	62.45	61.63	61.66	62.12	61.07	61.41	-	-
$\mathrm{GS}/^3\pi\pi^*$							-	-
$^{1}n\pi^{*}/^{3}n\pi^{*}$	0	0	0	0	0	0	0	0
$^{1}n\pi^{*}/^{3}\pi\pi^{*}$	44.68	43.8	43.92	44.13	43.36	51.48	45	54
				\mathbf{Aceto}	ne			
$\mathrm{GS}/^3n\pi^*$						59.28	-	-
$\mathrm{GS}/^3\pi\pi^*$						0.24	-	-
$^{1}n\pi^{*}/^{3}n\pi^{*}$						0.05	0	0
$\frac{1}{n\pi^*/3\pi\pi^*}$	43.75	43.18	43.36	43.47	42.72	50.57	44	54

^a1e-eff SOCC (B3LYP/TZVP)

^bfull Breit-Pauli SOCC (B3LYP/cc-pVTZ) using response theory

TABLE II: SOMF SOCCs in formal dehyde and acetone computed with TD-DFT/TDA (B3LYP, PBE0, ω PBEh, ω B97XD, and ω B97M-V) and EOM-EE-CCSD using aug-cc-pVTZ compared with values from Ref. 28.

Transition	B3LYP	PBE0	$\omega PBEh$	$\omega B97$	ω B97	EOM-EE-	B3LYP/	B3LYP/		
				X-D	M-V	CCSD	$PySOC^a$	$Dalton^{\hat{b}}$		
	Formaldehyde									
$\mathrm{GS}/^3n\pi^*$	60.62	60.00	60.03	60.67	59.25	59.52	-	-		
$\mathrm{GS}/^3\pi\pi^*$							-	-		
$^{1}n\pi^{*}/^{3}n\pi^{*}$	0	0	0	0	0	0	0	0		
$^{1}n\pi^{*}/^{3}\pi\pi^{*}$	44. 33	43.47	43.56	43.81	42.93	50.88	45	54		
				\mathbf{Aceto}	\mathbf{ne}					
$\mathrm{GS}/^3n\pi^*$						57.63	-	-		
$\mathrm{GS}/^3\pi\pi^*$						0.15	-	-		
$^{1}n\pi^{*}/^{3}n\pi^{*}$						0.01	0	0		
$\frac{1}{n}\pi^*/3\pi\pi^*$	43.08	42.71	42.96	43.07	42.16	49.92	44	54		

 a 1e-eff SOCC (B3LYP/TZVP)

^bfull Breit-Pauli SOCC (B3LYP/cc-pVTZ) using response theory

2. Biacetyl (BIA) and (2Z)-2-buten-2-ol (BOL)

Our next benchmark set comprises a diketone (BIA) and conjugated alcohol (BOL) previously studied by Carreras *et al.* using the RASCI and EOM-CCSD methods with SOMF approximation.⁴¹ Fig. 3 shows the relevant frontier MOs: π , n, and π^* . The LUMO in BIA and LUMO+1 in BOL are of π^* character, whereas the HOMO in BIA is of n type and in BOL it is of π character. Following this MO energy order, the lowest singlet and triplet states in BIA are of $n\pi^*$ character, in BOL, they are of $\pi\pi^*$ character.

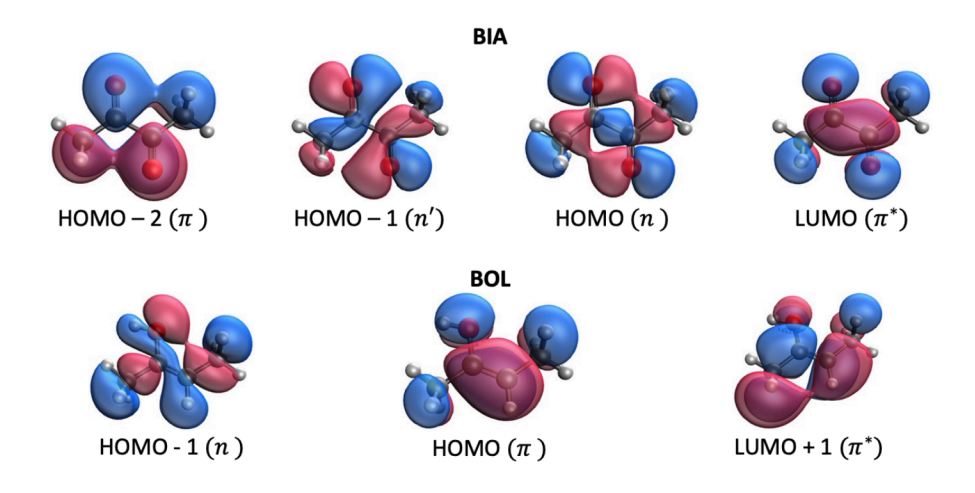


FIG. 3: Canonical Kohn-Sham molecular orbitals (π, n, π^*) of BIA and BOL; B3LYP/cc-pVTZ

Table S3 presents the vertical excitation energies, and NTO descriptors of low-lying singlet and triplet excited states computed using B3LYP/cc-pVTZ in BIA and BOL. Except for $\pi\pi^*$ state (S₉ state) of BIA for which PR_{NTO}=2.08, all other singlet and triplet states have PR_{NTO} close to 1, meaning that all computed excited states, except for S₉ in BIA, can be described by a single excitation. Table III shows the one-electron and SOMF SOCCs computed using B3LYP, comparing the results with EOM-CCSD and RASCI couplings.⁴¹ The trends in SOCCs follow El-Sayed's rules,^{78,79} featuring large SOCCs between states of different orbital characters, such as ${}^{1}\pi\pi^{*}/{}^{3}n\pi^{*}$ and ${}^{1}n\pi^{*}/{}^{3}\pi\pi^{*}$ transitions. In BIA, the SOMF SOCC between the ${}^{1}\pi\pi^{*}$ and ${}^{3}n\pi^{*}$ states computed with B3LYP differs by about 22 cm⁻¹ from those evaluated by the EOM-CCSD and RASCI methods. This can be explained by the different character of the S₉ state—at the B3LYP level, this state shows configuration mixing whereas the EOM-CCSD and RASCI wave-function retain pure ${}^{1}\pi\pi^{*}$ character. All other computed SOMF DFT couplings are within 6 cm⁻¹ from the EOM-CCSD SOMF couplings.

Overall, the SOCs computed with B3LYP show good agreement with the SOCs computed with EOM-EE-CCSD. The differences between RASCI and EOM-CCSD couplings observed in BOL can be attributed to insufficient treatment of dynamic correlation by RASCI.⁴¹

TABLE III: SOCC in BIA and BOL computed with TD-DFT/TDA (B3LYP/cc-pVTZ) compared with the EOM-CCSD and RASCI values.

Transition	B3LYF)	EOM - $CCSD^a$	$\overline{\mathrm{RASCI}^b}$					
	1e	SOMF	SOMF	SOMF					
BIA									
$\mathrm{GS}/^3n\pi^*$	0.00	0.00	0.00	0.00					
$GS/^3n'\pi^*$	130.31	82.05	85.79	81.25					
$\mathrm{GS}/^3\pi\pi^*$	0.00	0.00	0.00	0.00					
$^{1}n\pi^{*}/~^{3}n\pi^{*}$	1.01	0.66	0.17	0.16					
$^{1}n\pi^{*}/~^{3}n'\pi^{*}$	0.00	0.00	0.00	0.00					
$^{1}n\pi^{*}/~^{3}\pi\pi^{*}$	71.09	45.62	51.84	55.33					
$^{1}n'\pi^{*}/^{3}n\pi^{*}$	0.00	0.00	0.00	0.00					
$^{1}n'\pi^{*}/^{3}n'\pi^{*}$	0.68	0.43	0.02	0.45					
$^{1}n'\pi^{*}/^{3}\pi\pi^{*}$	0.00	0.00	0.00	0.00					
$^{1}\pi\pi^{*}/~^{3}n\pi^{*}$	33.65	21.72	44.19	44.6					
$^{1}\pi\pi^{*}/~^{3}n'\pi^{*}$	0.00	0.00	0.00	0.00					
$^{1}\pi\pi^{*}/~^{3}\pi\pi^{*}$	0.23	0.02	0.13	0.04					
		во	${f L}$						
$\mathrm{GS}/^3\pi\pi^*$	0.67	0.01	0.01	0.00					
$\mathrm{GS}/^3n\pi^*$	43.34	24.77	23.14	18.57					
$^{1}\pi\pi^{*}/~^{3}\pi\pi^{*}$	0.09	0.02	0.02	0.03					
$^{1}\pi\pi^{*}/~^{3}n\pi^{*}$	24.73	16.22	15.43	7.06					
$^{1}n\pi^{*}/~^{3}\pi\pi^{*}$	20.52	13.34	11.07	3.44					
$\frac{1}{n\pi^*/3n\pi^*}$	2.43	1.41	0.10	0.02					

^aEOM-CCSD/cc-pVTZ; from Ref. 41 ^bRASCI/cc-pVTZ; from Ref. 41

3. Psoralens

Psoralens are photosensitizers used in pharmaceutical applications.⁸⁰ They are naturally occurring in some plants, such as *Heracleum maximum* (commonly known as cow parsnip)⁸¹. Contained in the skin of the plant, psoralens are responsible for the ability of cow parsnip to cause skin rashes and blistering, initiated by sunlight (phytophotodermatitis). An important aspect of psoralens' pharmacological action is that it can react with DNA, and the reaction, initiated by UV light, proceeds in the triplet state.⁸²

SOCs in psoralen and its thio-derivatives (psoralenOO, psoralenOS, and psoralenSO) have been characterized theoretically in previous studies by Tatchen *et al.* (SOMF) using DFT/MRCI,⁸³ by Chiodo and Russo (full Breit-Pauli) using TD-DFT,²⁵ and, more recently, by Gao *et al.* (1e-eff) using TD-DFT and TD-DFTB,²⁸ and by Liu *et al.* (1e-eff) using OM2/CIS and TD-DFT.¹¹ Here, we use B3LYP/cc-pVDZ and compare the results with some of the previously available SOCCs between low-lying singlet and triplet states. Fig. 4 shows the frontier molecular orbitals involved in the low-lying excited states for psoralen compounds. In all three compounds, the HOMO-2 is of n type, HOMO-1 and HOMO are of π type, and LUMO, LUMO+1, and LUMO+2 are π^* orbitals

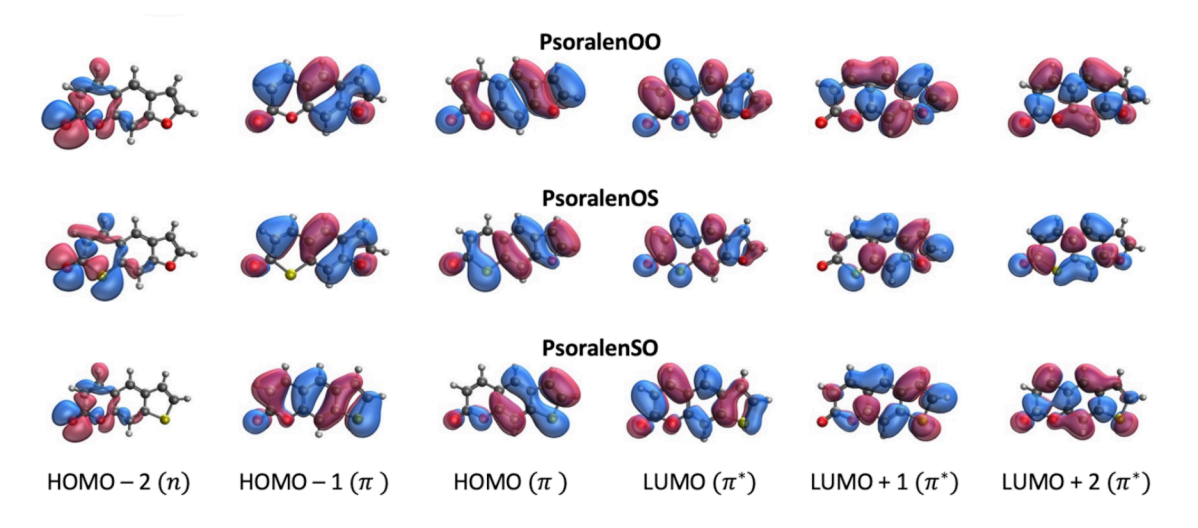


FIG. 4: Canonical Kohn-Sham molecular orbitals (π, n, π^*) of psoralen compounds; B3LYP/cc-pVDZ.

Tables S4 and S5 show the vertical excitation energies and NTO analysis of the lowlying singlet and triplet excited states. To make meaningful comparisons with previous studies^{25,28,83}, we carefully analyzed excited-state characters in our calculations. We found that the reported state numbering does not match ours—apparently, some states were missed in earlier studies. Tables S4 and S5 give the state labels from *Q-Chem* calculations, whereas in Table IV we give both sets of state labels.

TABLE IV: SOCCs in psoralen and its thio derivatives computed with B3LYP/cc-pVDZ and compared with previous calculations.

a with previous care	diadions.			
B3LYP		$\mathrm{DFT}/\mathrm{MRCI}^b$	$B3LYP^c$	$PBE0^d$
1el	SOMF	SOMF	1el-eff	full BP
		PsoralenOO		
$GS/T_1 1.60$	0.03	=	-	-
$GS/T_2 \ 0.24$	0.03	0.05	$1 (GS/T_1)$	$0.07 \; (GS/T_1)$
$GS/T_3 0.58$	0.05	-	-	-
$GS/T_4 66.09$	41.85	50.01	43	33.46
$S_1/T_2 = 0.97$	0.00	0.01	$1 (S_1/T_1)$	$0.08 (S_1/T_1)$
S_1/T_4 10.99	6.70	10.22	8	12.45
S_2/T_2 6.44	4.22	28.1	$19 (S_3/T_1)$	$9.96 (S_2/T_1)$
		PsoralenOS		
GS/T_1 1.31	0.01	-	-	-
GS/T_2 0.25	0.02	0.04	$1 (GS/T_1)$	$0.05 \; (GS/T_1)$
$GS/T_3 99.15$	69.48	78.53	$70 \; (GS/T_4)$	$71.45 (GS/T_4)$
$GS/T_4 0.69$	0.30	-	-	-
S_1/T_2 1.01	0.00	0.04	$0 (S_1/T_1)$	$0.08 (S_1/T_1)$
S_1/T_3 38.13	34.51	35.6	$37 (S_1/T_4)$	$45 (S_1/T_4)$
S_2/T_2 35.36	27.49	11.13	$10 (S_2/T_1)$	$22.81 (S_2/T_1)$
		PsoralenSO		
GS/T_1 1.12	0.13	0.04	0	0.03
GS/T_2 1.18	0.22	-	-	_
$GS/T_3 0.74$	0.20	-	-	-
$GS/T_4 64.76$	40.89	49.44	$42 \; (GS/T_5)$	31.70
S_1/T_1 1.03	0.03	0.01	1	0.08
S_1/T_4 6.34	4.12	6.21	$4 (S_1/T_5)$	
S_3/T_1 28.00	17.93	25.88	16	$13.74 (S_2/T_1)$

^bDFT-MRCI/TZVP; Ref. 83

Table IV shows the 1el and SOMF SOCCs for psoralen compounds. For all three psoralen molecules, most of the computed SOMF SOCCs agree with the 1e-eff-B3LYP values (computed with PySOC) within 3 cm⁻¹. Only the S_2/T_2 couplings in psoralenOO and psoralenOS show the largest deviation from the 1e-eff treatment, but agree well with the full Breit-Pauli treatment. For the larger SOCCs that are greater than 1 cm⁻¹, DFT/MRCI val-

 $[^]c 1 \mathrm{e\textsc{-}eff}$ SOCC with TD-DFT/B3LYP/TZVP, Ref. 28; reported state labels are given in parenthesis

^dfull Breit-Pauli SOCC with TD-DFT/PBE0/TZVP, Ref. 25; reported state labels are given in parenthesis

ues are larger than our SOMF B3LYP values, while the couplings that are less than 1 cm⁻¹ agree within 0.1 cm⁻¹. While the couplings between the ground state and excited triplets are typically overestimated in this work with respect to the full Breit-Pauli treatment (computed with *MolSOC*), those between singlet and triplet excited states are usually smaller. Overall, we observe a good qualitative agreement between our values and the SOCCs computed with previous studies.

B. Spin-orbit couplings calculated with SF-TD-DFT

1.
$$CH_2$$
, NH_2^+ , SiH_2 , and PH_2^+

In these molecules, the description of the low-lying states using standard Kohn-Sham DFT and TD-DFT is inadequate because of the diradical character of the singlet states⁸⁴. This problem can be circumvented by using SF-TD-DFT with a high-spin triplet reference⁵⁵. In contrast to other types of organic diradicals, methylene-like diradicals are highly sensitive to the functional employed, as documented in previous SF-TD-DFT studies^{51,54}. Specifically, only non-collinear SF-TD-DFT (NC-SF-TD-DFT) can yield accurate results for these species, and only with functionals that do not use Becke's exchange. The best results were obtained with the functionals from the PBE family. Benchmark calculations on other classes of molecules have also shown superior performance of NC-SF-TD-DFT with PBE0 and ω PBEh.^{58,62} Following previous studies,^{35,36,41} we computed SOCCs between the lowest triplet (3 B₂) and singlet (1 A₁) states of these diradicals (CH₂, NH₂⁺, SiH₂, and PH₂⁺). We used NC-SF-TD-DFT and considered B3LYP, PBE0, ω PBEh, ω B97X-D, and ω B97M-V.

TABLE V: SOCCs (cm⁻¹) between ${}^{3}B_{2}$ and ${}^{1}A_{1}$ states in CH₂, NH₂⁺, SiH₂, and PH₂⁺ computed using SOMF with NC-SF-TD-DFT.

$Method^a$	CH_2	NH_2^+	SiH_2	PH_2^+			
PBE0	10.36	15.15	68.67	135.38			
$\omega \mathrm{PBEh}$	10.32	15.03	68.93	135.66			
B3LYP	12.29	19.83	75.69	150.12			
$\omega \mathrm{B}97\mathrm{x-D}$	12.85	18.11	75.20	157.21			
$\omega \mathrm{B97M-V}$	13.16	20.20	79.73	155.90			
EOM-SF-CCSD b	10.86	18.26	56.74	119.97			
^a cc-pVTZ basis							
b From Ref. 36							

Table V presents the SOMF SOCCs in these diradicals using NC-SF-TD-DFT, com-

paring them with SOMF SOCCs obtained with EOM-SF-CCSD.³⁶ In contrast to TD-DFT calculations of formaldehyde and acetone discussed above, here we observed a strong functional dependence, with PBE0 and ω PBEh performing similarly and B3LYP, ω B97x-D, and ω B97M-V showing small differences in couplings with each other. For CH₂, SiH₂, and PH₂⁺, PBE0 and ω PBEh compare well with EOM-SF-CCSD, with differences increasing with an increase in atomic number, 0.5 cm⁻¹ in the case of CH₂⁺ and 16 cm⁻¹ in the case of PH₂⁺. Overall, we confirm previous recommendation⁵⁴ to use PBE0 and ω PBEh in NC-SF-TD-DFT calculations—as these functionals yield accurate estimates of both energy differences between the states and the respective SOCCs.

2. BH, AlH, HSiF, HSiCl, HSiBr

Next, we consider closed-shell molecules with moderate diradical character, BH, AlH, HSiF, HSiCl, and HSiBr, previously studied by Christiansen *et al.* using linear response CCSD (LR-CCSD, equivalent to EOM-EE-CCSD for the energies and slightly different for properties) and Epifanovsky *et al.* using EOM-SF-CCSD/EOM-EE-CCSD methods.^{32,35} Here, we consider SOCs between the $1^1\Sigma^+$ and $1^3\Pi$ states for BH, AlH, and between $1^1A'$ and $1^3A''$ states for silylenes HSiX, X = F, Cl, Br. We use NC-SF-TD-DFT with PBE0/cc-pCVTZ and ω PBEh/cc-pCVTZ. Table V shows the results for these molecules. As one can see, there is an excellent agreement between SOCCs computed using PBE0/ ω PBEh and EOM-SF-CCSD, with differences less than 3 cm⁻¹ (except for HSiBr for which we observe 15 cm⁻¹ and 31 cm⁻¹ difference between PBE0 and ω PBEh with EOM-SF-CCSD respectively). Similarly, there is a good agreement between the SOCCs computed with LR-CCSD and PBE0/ ω PBEh.

3. Spin reversal energy barrier in Fe(III) SMM

Finally, we consider a mononuclear Fe(III) SMM, (PMe₃)Fe(III)Cl₃, which is reported to have the highest effective energy barrier $U_{eff} = 81 \text{ cm}^{-1}$ among Fe(III)-based SMMs.⁶⁹ This energy barrier for spin inversion arises because of the splitting of the ground state due to SOC. The experimental spin-reversal barrier is U = 100, as computed from the magnetic anisotropy ($D = -50 \text{ cm}^{-1}$) and ground-state spin (S = 3/2), with $U = |D|(S^2 - 10^{-1})$

TABLE VI: SOCCs (cm⁻¹) in BH, AlH, HSiF, HSiCl, and HSiBr computed using SOMF with NC-SF-TD-DFT (PBE0/ ω PBEh;cc-pcVTZ).

Method	ВН	AlH	HSiF	HSiCl	HSiBr
	$1^{1}\Sigma^{+}/\ 1^{3}\Pi$	$1^1\Sigma^+/1^3\Pi$	$1^1 A' / 1^3 A''$	$1^1 A' / 1^3 A''$	$1^1 A' / 1^3 A''$
PBE0	4.39	34.98	79.52	106.85	267.78
$\omega \mathrm{PBEh}$	4.41	35.17	79.87	105.47	252.40
EOM-SF-CCSD a	4.10	32.94	78.28	108.43	283.47
$LR-CCSD^b$	3.48^{c}	27.06^{c}	71.10^{d}	99.38^{d}	270.93^d

 a EOM-CCSD/cc-pCVTZ, from Ref. 35 b LR-CCSD, from Ref. 32 c aug-cc-pVTZ d ANO2 basis.

1/4).⁶⁹ Alessio and Krylov used the EOM-SF-CCSD treatment to calculate the spin reversal energy barrier and magnetic properties of this complex.⁸⁵ Following this study, here we compute the energy barrier using the spin-orbit coupling obtained with SOMF NC-SF-TD-DFT treatment.

TABLE VII: Energy gaps (ΔE , in cm⁻¹) and $\langle S^2 \rangle$ of the target spin-flip states obtained from the high spin hextet reference state computed with PBE0, ω PBEh/cc-pVDZ.

		Ref	SF_1	SF_2	SF_3	SF_4	SF_5
PBE0	$< S^2 >$	8.76	3.84	3.85	8.74	3.83	3.82
	$\Delta \mathrm{E}$	-	0	398	553	4122	4471
$\omega \mathrm{PBEh}$	$< S^2 >$	8.76	3.82	3.82	8.77	3.81	3.82
	$\Delta \mathrm{E}$	-	0	344	715	4116	4495
EOM -SF-CCSD a	$< S^2 >$	8.75	3.81	3.81	8.73	3.83	3.83
	$\Delta \mathrm{E}$	-	0	92	2074	7245	7447

^aEOM-SF-CCSD/cc-pVDZ, from Ref. 85.

For this complex, we use PBE0 and ω PBEh functionals to access the quartet ground state (S = 3/2) and other closely lying excited states by spin-flip excitations from a high-spin reference of S = 5/2. We obtain three spin-flip states (see Table VII) lying within 715 cm⁻¹; SF₁ and SF₂ are quartet states while SF₃ is a hextet state. This differs from the EOM-SF-CCSD results, where SF₃ is about 2000 cm⁻¹ above SF₂.⁸⁵ We then proceed to compute the spin reversal energy barrier with 2, 3, and 5 low-lying SF states by including the SOC effects using the state-interaction procedure.³⁶ The inclusion of only two states is insufficient to characterize the energy barrier with SF-TD-DFT (see Table VIII), however, the energy barrier calculated with 3 states gives a value of 97 (PBE0) cm⁻¹ and 100 (ω PBEh) cm⁻¹, in excellent agreement with the experimental estimate of 100 cm⁻¹. The energy barrier

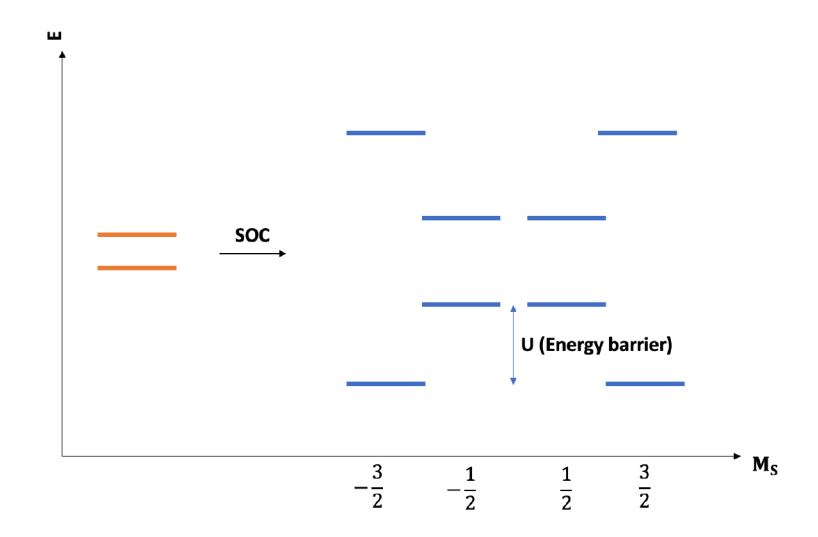


FIG. 5: Energy levels arising from the splitting of two lowest SF states induced by SOC.

computed with EOM-SF-CCSD converges to 130 cm⁻¹ with the inclusion of 5 states. To assess the effects of energy gaps of the SF states, we computed the energy barrier using PBE0 SOCs and EOM-SF-CCSD energy gaps (denoted as EOM/PBE0 in Table VIII). This combined EOM/PBE0 calculation gives energy barriers close to the EOM-SF-CCSD results. Therefore, we conclude that the differences in energy barriers computed using PBE0/ ω PBEh and EOM-SF-CCSD result from the different energy gaps of the SF states predicted by these methods.

TABLE VIII: Energy barrier U (cm⁻¹) computed using 2, 3, and 5 lowest SF states in trigonal bipyramidal (PMe₃)Fe(III)Cl₃ complex with NC-SF-DFT/PBE0/cc-pVDZ.

No. of states	s PBE0	$\omega PBEh$	EOM-SF-CCSD b	$EOM/PBE0^c$	$\operatorname{Exp-U}^d$
2	52	59	103	99	
3	97	100	130	119	
5	94	92	128	117	100

^bEOM-SF-CCSD, Ref. 85

^cEnergy barrier calculated with EOM-SF-CCSD energies and PBE0 SOCs ^dexperimental value, Ref. 69

V. CONCLUSIONS

We presented the implementation of SOCs with TD-DFT and SF-TD-DFT and benchmark calculations for several organic molecules of a closed-shell character as well as diradicals and one SMM. The algorithm is based on evaluating matrix elements of the Breit-Pauli

operator by the application of Wigner–Eckart's theorem to reduced one-particle density matrices. We used NTO analysis to characterize the nature of the interacting states. We tested functional and basis set dependencies for formaldehyde and acetone with TD-DFT using B3LYP, PBE0, LRC- ω PBEh, ω B97X-D, and ω B97M-V functionals and the cc-pVTZ and aug-cc-pVTZ basis sets. The results demonstrate that SOCCs are rather insensitive to the choice of functionals and basis sets, with a variation of less than 2 cm⁻¹. In agreement with El-Sayed's rules, SOCs are large for transitions involving a change of the orbital type. We validated our SOMF SOCC results by comparisons with the reference values from TD-DFT, EOM-EE-CCSD, RASCI, DFT/MRCI, EOM-SF-CCSD, and LR-CCSD studies. Calculations for diradicals with NC-SF-TD-DFT show strong functional dependencies, with PBE0 and $\omega PBEh$ performing similar to EOM-SF-CCSD, and B3LYP, $\omega B97X-D$, and $\omega B97M-$ V performing similar to each other; this is in agreement with previous benchmark studies in which energy gaps and state characters were considered. 54,86 Using the state-interaction approach, we computed the spin-reversal energy barrier in Fe(III) SMM with PBE0 and LRC- ω PBEh, which matches the experimental estimate when the three lowest SF states are included in the calculation.

This new implementation extends the scope of computational tools for modeling spinforbidden processes in large molecular systems, as illustrated by our recent study in which we applied this SF-TD-DFT SOC code to describe the magnetic behavior of nickelocene molecular magnet adsorbed on the MgO(001) surfaces using the state-interaction scheme.⁵⁹

Acknowledgments

This work is supported by the National Science Foundation through "CCI Phase I: NSF Center for Advanced Molecular Architectures for Quantum Information Science" (Award CHE20223563).

The authors declare the following competing financial interest(s): A.I.K. is the president and a part-owner of Q-Chem, Inc.

Data availability

The data that support the findings of this study are available within the article and the associated SI.

- [1] J. N. Harvey, Understanding the kinetics of spin-forbidden chemical reactions, Phys. Chem. Chem. Phys. **2007**, 331 (2006).
- [2] F. Neese and D. A. Pantazis, What is not required to make a single molecule magnet, Faraday Discuss. 148, 229 (2011).
- [3] J. D. Rinehart and J. R. Long, Exploiting single-ion anisotropy in the design of f-element single-molecule magnets, Chem. Sci. 2, 2078 (2011).
- [4] A. Bergantini, M. J. Abplanalp, P. Pokhilko, A. I. Krylov, C. N. Shingledecker, E. Herbst, and R. I. Kaiser, A combined experimental and theoretical study on the formation of interstellar propylene oxide (CH₃CHCH₂O) - a chiral molecule, Astrophys. J. 860, 108 (2018).
- [5] Q. Ou and J. E. Subotnik, Electronic relaxation in benzaldehyde evaluated via TD-DFT and localized diabatization: Intersystem crossings, conical intersections, and phosphorescence, J. Phys. Chem. C 117, 9839 (2013).
- [6] P. Pokhilko, R. Shannon, D. Glowacki, H. Wang, and A. I. Krylov, Spin-forbidden channels in reactions of unsaturated hydrocarbons with O(³P), J. Phys. Chem. A **123**, 482 (2019).
- [7] B. F. Habenicht and O. V. Prezhdo, Ab initio time-domain study of the triplet state in a semiconducting carbon nanotube: intersystem crossing, phosphorescence time, and line width, J. Am. Chem. Soc. 134, 15648 (2012).
- [8] L. Favero, G. Granucci, and M. Persico, Dynamics of acetone photodissociation: a surface hopping study, Phys. Chem. Chem. Phys. **15**, 20651 (2013).
- [9] B. Fu, B. C. Shepler, and J. M. Bowman, Three-state trajectory surface hopping studies of the photodissociation dynamics of formaldehyde on ab initio potential energy surfaces, J. Am. Chem. Soc. 133, 7957 (2011).
- [10] G. Cui and W. Thiel, Generalized trajectory surface-hopping method for internal conversion and intersystem crossing, J. Chem. Phys. 141, 124101 (2014).
- [11] J. Liu, Z. Lan, and J. Yang, An efficient implementation of spin-orbit coupling within the framework of semiempirical orthogonalization-corrected methods for ultrafast intersystem crossing dynamics, Phys. Chem. Chem. Phys. 23, 22313 (2021).
- [12] P. K. Samanta, D. Kim, V. Coropceanu, and J.-L. Brédas, Up-conversion intersystem crossing rates in organic emitters for thermally activated delayed fluorescence: Impact of the nature

- of singlet vs triplet excited states, J. Am. Chem. Soc. 139, 4042 (2017).
- [13] Z. Tu, F. Wang, and X. Li, Equation-of-motion coupled-cluster method for ionized states with spin-orbit coupling, J. Chem. Phys. **136**, 174102 (2012).
- [14] Z. Wang, S. Hu, F. Wang, and J. Guo, Equation-of-motion coupled-cluster method for doubly ionized states with spin-orbit coupling, J. Chem. Phys. 142, 144109 (2015).
- [15] A. Asthana, J. Liu, and L. Cheng, Exact two-component equation-of-motion coupled-cluster singles and doubles method using atomic mean-field spin-orbit integrals, J. Chem. Phys. 150, 074102 (2019).
- [16] J. Liu, Y. Shen, A. Asthana, and L. Cheng, Two-component relativistic coupled-cluster methods using mean-field spin-orbit integrals, J. Chem. Phys. 148, 034106 (2018).
- [17] J. Liu and L. Cheng, An atomic mean-field spin-orbit approach within exact two-component theory for a non-perturbative treatment of spin-orbit coupling, J. Chem. Phys. 148, 144108 (2018).
- [18] M. Guo, Z. Wang, and F. Wang, Equation-of-motion coupled-cluster theory for double electron attachment with spin-orbit coupling, J. Chem. Phys. 153, 214118 (2020).
- [19] D. G. Fedorov, S. Koseki, M. W. Schmidt, and M. S. Gordon, Spin-orbit coupling in molecules: Chemistry beyond the adiabatic approximation, Int. Rev. Phys. Chem. 22, 551 (2003).
- [20] C. M. Marian, Spin-orbit coupling and intersystem crossing in molecules, WIREs Comput. Mol. Sci. 2, 187 (2012).
- [21] B. A. Hess, C. M. Marian, U. Wahlgren, and O. Gropen, A mean-field spin-orbit method applicable to correlated wavefunctions, Chem. Phys. Lett. 251, 365 (1996).
- [22] J. Tatchen and C. M. Marian, On the performance of approximate spin-orbit hamiltonians in light conjugated molecules: the fine-structure splitting of HC₆H⁺, NC₅H⁺, and NC₄N⁺, Chem. Phys. Lett. 313, 351 (1999).
- [23] D. Danovich, C. M. Marian, T. Neuheuser, S. D. Peyerimhoff, and S. Shaik, Spin-orbit coupling patterns induced by twist and pyramidalization modes in C₂H₄: A quantitative study and a qualitative analysis, J. Phys. Chem. A 102, 5923 (1998).
- [24] F. Neese, Efficient and accurate approximations to the molecular spin-orbit coupling operator and their use in molecular g-tensor calculations, J. Chem. Phys. **122**, 034107 (2005).
- [25] S.G. Chiodo and N. Russo, DFT spin-orbit coupling between singlet and triplet excited states: A case of psoralen compounds, Chem. Phys. Lett. 490, 90 (2010).

- [26] Z. Li, B. Suo, Y. Zhang, Y. Xiao, and W. Liu, Combining spin-adapted open-shell TD-DFT with spin-orbit coupling, Mol. Phys. 111, 3741 (2013).
- [27] F. Franco de Carvalho, B. F. E. Curchod, T. J. Penfold, and I. Tavernelli, Derivation of spin-orbit couplings in collinear linear-response TDDFT: A rigorous formulation, J. Chem. Phys. 140, 144103 (2014).
- [28] X. Gao, S. Bai, D. Fazzi, T. Niehaus, M. Barbatti, and W. Thiel, Evaluation of spin-orbit couplings with linear-response time-dependent density functional methods, J. Chem. Theory Comput. 13, 515 (2017).
- [29] F. Dinkelbach, M. Kleinschmidt, and C. M. Marian, Assessment of interstate spin-orbit couplings from linear response amplitudes, J. Chem. Theory Comput. 13, 749 (2017).
- [30] M. Kleinschmidt, J. Tatchen, and C. M. Marian, Spin-orbit coupling of DFT/MRCI wavefunctions: Method, test calculations, and application to thiophene, J. Comput. Chem. 23, 824 (2002).
- [31] M. Kleinschmidt and C. M. Marian, Efficient generation of matrix elements for one-electron spin-orbit operators, Chem. Phys. **311**, 71 (2005).
- [32] O. Christiansen, J. Gauss, and B. Schimmelpfennig, Spin-orbit coupling constants from coupled-cluster response theory, Phys. Chem. Chem. Phys. 2, 965 (2000).
- [33] K. Klein and J. Gauss, Perturbative calculation of spin-orbit splittings using the equation-of-motion ionization-potential coupled-cluster ansatz, J. Chem. Phys. **129**, 194106 (2008).
- [34] D. Bokhan, A. Perera, D. N. Trubnikov, and R. J. Bartlett, Excitation energies with spin-orbit couplings using equation-of-motion coupled-cluster singles and doubles eigenvectors, J. Chem. Phys. 147, 164118 (2017).
- [35] E. Epifanovsky, K. Klein, S. Stopkowicz, J. Gauss, and A. I. Krylov, Spin-orbit couplings within the equation-of-motion coupled-cluster framework: Theory, implementation, and benchmark calculations, J. Chem. Phys. 143, 064102 (2015).
- [36] P. Pokhilko, E. Epifanovsky, and A. I. Krylov, General framework for calculating spin-orbit couplings using spinless one-particle density matrices: theory and application to the equationof-motion coupled-cluster wave functions, J. Chem. Phys. 151, 034106 (2019).
- [37] L.A. Mück and J. Gauss, Spin-orbit splittings in degenerate open-shell states via Mukherjee's multireference coupled-cluster theory: A measure for the coupling contribution, J. Chem. Phys. 136, 111103 (2012).

- [38] D. G. Fedorov and M. S. Gordon, A study of the relative importance of one and two-electron contributions to spin-orbit coupling, J. Chem. Phys. **112**, 5611 (2000).
- [39] S. Koseki, N. Matsunaga, T. Asada, M. W. Schmidt, and M. S. Gordon, Spin-orbit coupling constants in atoms and ions of transition elements: Comparison of effective core potentials, model core potentials, and all-electron methods, J. Phys. Chem. A 123, 2325 (2019).
- [40] P. Å. Malmqvist, B. O. Roos, and B. Schimmelphennig, The restricted active space (RAS) state interaction approach with spin-orbit coupling, Chem. Phys. Lett. **357**, 230 (2002).
- [41] A. Carreras, H. Jiang, P. Pokhilko, A.I. Krylov, P. M. Zimmerman, and D. Casanova, Calculation of spin-orbit couplings using RASCI spinless one-particle density matrices: Theory and applications, J. Chem. Phys. 153, 214107 (2020).
- [42] A. Berning, M. Schweizer, H.-J. Werner, P. Knowles, and P. Palmieri, Spin-orbit matrix elements for internally contracted multireference configuration interaction wavefunctions, Mol. Phys. 98, 1823 (2000).
- [43] M. Roemelt, Spin orbit coupling for molecular ab initio density matrix renormalization group calculations: Application to g-tensors, J. Chem. Phys. **143**, 044112 (2015).
- [44] E. R. Sayfutyarova and G. K. L. Chan, A state interaction spin-orbit coupling density matrix renormalization group method, J. Chem. Phys. **144**, 234301 (2016).
- [45] C. Eckart, The application of group theory to the quantum dynamics of monatomic systems, Rev. Mod. Phys. 2, 305 (1930).
- [46] E. Wigner, Einige Folgerungen aus der Schrödingerschen Theorie für die Termstrukturen, Zeits. f. Physik 43, 624 (1927).
- [47] R.N. Zare, Angular momentum: understanding spatial aspects in chemistry and physics. J. Wiley & Sons, 1988.
- [48] M. L. Vidal, P. Pokhilko, A. I. Krylov, and S. Coriani, Equation-of-motion coupled-cluster theory to model L-edge x-ray absorption and photoelectron spectra, J. Phys. Chem. Lett. 11, 8314 (2020).
- [49] O. R. Meitei, S. E. Houck, and N. J. Mayhall, Spin-orbit matrix elements for a combined spin-flip and IP/EA approach, **16**, 3597 (2020).
- [50] M. E. Casida, Time-dependent density-functional theory for molecules and molecular solids,J. Molec. Struct. (THEOCHEM) 914, 3 (2009).
- [51] Y. Shao, M. Head-Gordon, and A. I. Krylov, The spin-flip approach within time-dependent

- density functional theory: Theory and applications to diradicals, J. Chem. Phys. **118**, 4807 (2003).
- [52] F. Wang and T. Ziegler, Time-dependent density functional theory based on a noncollinear formulation of the exchange-correlation potential, J. Chem. Phys. **121**, 12191 (2004).
- [53] Z. Rinkevicius, O. Vahtras, and H. Årgen, Spin-flip time dependent density functional theory applied to excited states with single, double, or mixed electron excitaion character, J. Chem. Phys. 133, 114104 (2010).
- [54] Y. A. Bernard, Y. Shao, and A. I. Krylov, General formulation of spin-flip time-dependent density functional theory using non-collinear kernels: Theory, implementation, and benchmarks, J. Chem. Phys. 136, 204103 (2012).
- [55] D. Casanova and A. I. Krylov, Spin-flip methods in quantum chemistry, Phys. Chem. Chem. Phys. **22**, 4326 (2020).
- [56] S. Hirata and M. Head-Gordon, Time-dependent density functional theory within the Tamm-Dancoff approximation, Chem. Phys. Lett. **314**, 291 (1999).
- [57] N. J. Mayhall and M. Head-Gordon, Computational quantum chemistry for multiple-site Heisenberg spin couplings made simple: Still only one spin-flip required, J. Phys. Chem. Lett. 6, 1982 (2015).
- [58] S. Kotaru, S. Kähler, M. Alessio, and A. I. Krylov, Magnetic exchange interactions in binuclear and tetranuclear iron(III) complexes described by spin-flip DFT and Heisenberg effective Hamiltonians, J. Comput. Chem. (2022), in press, https://doi.org/10.1002/jcc.26941.
- [59] M. Alessio, S. Kotaru, G. Giudetti, and A. I. Krylov, Origin of magnetic anisotropy in nickelocene molecular magnet and resilience of its magnetic behavior, J. Phys. Chem. C (2022), submitted; https://chemrxiv.org/engage/chemrxiv/article-details/630057d40c5277d5cebb8768.
- [60] E. Epifanovsky, T. B. Gilbert, X. Feng, J. Lee, Y. Mao, N. Mardirossian, P. Pokhilko, A. F. White, M. P. Coons, A. L. Dempwolff, Z. Gan, D. Hait, P. R. Horn, L. D. Jacobson, I. Kaliman, J. Kussmann, A. W. Lange, K. U. Lao, D. S. Levine, J. Liu, S. C. McKenzie, A. F. Morrison, K. D. Nanda, F. Plasser, D. R. Rehn, M. L. Vidal, Z.-Q. You, Y. Zhu, B. Alam, B. J. Albrecht, A. Aldossary, E. Alguire, J. H. Andersen, V. Athavale, D. Barton, K. Begam, A. Behn, N. Bellonzi, Y. A. Bernard, E. J. Berquist, H. G. A. Burton, A. Carreras, K. Carter-Fenk, R. Chakraborty, A. D. Chien, K. D. Closser, V. Cofer-Shabica, S. Dasgupta, M. de Wergifosse, J. Deng, M. Diedenhofen, H. Do, S. Ehlert, P.-T. Fang, S. Fatehi, Q. Feng,

- T. Friedhoff, J. Gayvert, Q. Ge, G. Gidofalvi, M. Goldev, J. Gomes, C. E. González-Espinoza, S. Gulania, A. O. Gunina, M. W. D. Hanson-Heine, P. H. P. Harbach, A. Hauser, M. F. Herbst, M. Hernández Vera, M. Hodecker, Z. C. Holden, S. Houck, X. Huang, K. Hui, B. C. Huynh, M. Ivanov, A. Jász, H. Ji, H. Jiang, B. Kaduk, S. Kähler, K. Khistyaev, J. Kim, G. Kis, P. Klunzinger, Z. Koczor-Benda, J. H. Koh, D. Kosenkov, L. Koulias, T. Kowalczyk, C. M. Krauter, K. Kue, A. Kunitsa, T. Kus, I. Ladjánszki, A. Landau, K. V. Lawler, D. Lefrancois, S. Lehtola, R. R. Li, Y.-P. Li, J. Liang, M. Liebenthal, H.-H. Lin, Y.-S. Lin, F. Liu, K.-Y. Liu, M. Loipersberger, A. Luenser, A. Manjanath, P. Manohar, E. Mansoor, S. F. Manzer, S.-P. Mao, A. V. Marenich, T. Markovich, S. Mason, S. A. Maurer, P. F. McLaughlin, M. F. S. J. Menger, J.-M. Mewes, S. A. Mewes, P. Morgante, J. W. Mullinax, K. J. Oosterbaan, G. Paran, A. C. Paul, S. K. Paul, F. Pavošević, Z. Pei, S. Prager, E. I. Proynov, A. Rák, E. Ramos-Cordoba, B. Rana, A. E. Rask, A. Rettig, R. M. Richard, F. Rob, E. Rossomme, T. Scheele, M. Scheurer, M. Schneider, N. Sergueev, S. M. Sharada, W. Skomorowski, D. W. Small, C. J. Stein, Y.-C. Su, E. J. Sundstrom, Z. Tao, J. Thirman, G. J. Tornai, T. Tsuchimochi, N. M. Tubman, S. P. Veccham, O. Vydrov, J. Wenzel, J. Witte, A. Yamada, K. Yao, S. Yeganeh, S. R. Yost, A. Zech, I. Y. Zhang, X. Zhang, Y. Zhang, D. Zuev, A. Aspuru-Guzik, A. T. Bell, N. A. Besley, K. B. Bravaya, B. R. Brooks, D. Casanova, J.-D. Chai, S. Coriani, C. J. Cramer, G. Cserey, A. E. DePrince, R. A. DiStasio, A. Dreuw, B. D. Dunietz, T. R. Furlani, W. A. Goddard, S. Hammes-Schiffer, T. Head-Gordon, W. J. Hehre, C.-P. Hsu, T.-C. Jagau, Y. Jung, A. Klamt, J. Kong, D. S. Lambrecht, W. Liang, N. J. Mayhall, C. W. McCurdy, J. B. Neaton, C. Ochsenfeld, J. A. Parkhill, R. Peverati, V. A. Rassolov, Y. Shao, L. V. Slipchenko, T. Stauch, R. P. Steele, J. E. Subotnik, A. J. W. Thom, A. Tkatchenko, D. G. Truhlar, T. Van Voorhis, T. A. Wesolowski, K. B. Whaley, H. L. Woodcock, P. M. Zimmerman, S. Faraji, P. M. W. Gill, M. Head-Gordon, J. M. Herbert, and A. I. Krylov, Software for the frontiers of quantum chemistry: An overview of developments in the Q-Chem 5 package, J. Chem. Phys. **155**, 084801 (2021).
- [61] A. I. Krylov and P. M. W. Gill, Q-Chem: An engine for innovation, WIREs: Comput. Mol. Sci. 3, 317 (2013).
- [62] N. Orms and A. I. Krylov, Singlet-triplet energy gaps and the degree of diradical character in binuclear copper molecular magnets characterized by spin-flip density functional theory, Phys. Chem. Chem. Phys. 20, 13127 (2018).

- [63] H. A. Bethe and E. E. Salpeter, Quantum mechanics of one and two electron atoms. Plenum, New York, 1977.
- [64] P. Schwerdtfeger, editor, Relativistic Electronic Structure Theory. Elsevier, Amsterdam, 2002.
- [65] C.D. Sherrill, M.L. Leininger, T.J. Van Huis, and H.F. Schaefer III, Structures and vibrational frequencies in the full configuration interaction limit: Predictions for four electronic states of methylene using triple-zeta plus double polarization (TZ2P) basis, J. Chem. Phys. 108, 1040 (1998).
- [66] J.C. Stefens, Y. Yamaguchi, C.D. Sherrill, and H.F. Schaefer III, The \tilde{X}^3 B₁, \tilde{a}^1 A₁, \tilde{b}^1 B₁, and $\tilde{c}^1\Sigma_g^+$ electronic states of NH₂⁺, J. Phys. Chem. **102**, 3999 (1998).
- [67] Y. Yamaguchi, T.J. Van Huis, C.D. Sherrill, and H.F. Schaefer III, The $\tilde{X}^1 A_1$, $\tilde{a}^3 B_1$, $\tilde{A}^1 B_1$ and $\tilde{B}^1 A_1$ electronic states of SiH₂, Theor. Chem. Acc. **97**, 341 (1997).
- [68] T.J. Van Huis, Y. Yamaguchi, C.D. Sherrill, and H.F. Schaefer III, The $\tilde{X}^1 A_1$, $\tilde{a}^3 B_1$, $\tilde{A}^1 B_1$ and $\tilde{B}^1 A_1$ electronic states of PH₂⁺, J. Phys. Chem. **101**, 6955 (1997).
- [69] X. Feng, S. J. Hwang, J.-L. Liu, Y.-C. Chen, M.-L. Tong, and D. G. Nocera, Slow magnetic relaxation in intermediate spin S = 3/2 mononuclear Fe(III) complexes, J. Am. Chem. Soc. 139, 16474 (2017).
- [70] A.D. Becke, Density-functional thermochemistry. III. The role of exact exchange, J. Chem. Phys. 98, 5648 (1993).
- [71] C. Adamo and V. Barone, Toward reliable density functional methods without adjustable parameters: The PBE0 model, J. Chem. Phys. **110**, 6158 (1999).
- [72] M.A. Rohrdanz, K.M. Martins, and J.M. Herbert, A long-range-corrected density functional that performs well for both ground-state properties and time-dependent density functional theory excitation energies, including charge-transfer excited states, J. Chem. Phys. 130, 054112 (2009).
- [73] J.-D. Chai and M. Head-Gordon, Long-range corrected hybrid density functionals with damped atom-atom dispersion interactions, Phys. Chem. Chem. Phys. **10**, 6615 (2008).
- [74] N. Mardirossian and M. Head-Gordon, ω B97M-V: A combinatorially optimized, range-separated hybrid, meta-GGA density functional with VV10 nonlocal correlation, J. Chem. Phys. **144**, 214110 (2016).
- [75] F. Plasser, M. Wormit, and A. Dreuw, New tools for the systematic analysis and visualization of electronic excitations. I. Formalism, J. Chem. Phys. 141, 024106 (2014).

- [76] S. Mewes, F. Plasser, A. Krylov, and A. Dreuw, Benchmarking excited-state calculations using exciton properties, J. Chem. Theory Comput. 14, 710 (2018).
- [77] P. Pokhilko and A. I. Krylov, Quantitative El-Sayed rules for many-body wavefunctions from spinless transition density matrices, J. Phys. Chem. Lett. 10, 4857 (2019).
- [78] M. A. El-Sayed, Spin-orbit coupling and the radiationless processes in nitrogen heterocycles, J. Chem. Phys. 38, 2834 (1963).
- [79] M. A. El-Sayed, Triplet state: Its radiative and non-radiative properties, Acc. Chem. Res. 1, 8 (1968).
- [80] P. S. Song and K. J. Tapley, Photochemistry and photobiology of psoralens, Photochem. and Photobiol. 29, 1177 (1979).
- [81] https://en.wikipedia.org/wiki/Heracleum_maximum; accessed 10/05/2022.
- [82] J. Diekmann, J. Gontcharov, S. Fröbel, C. T. Ziegenbein, W. Zinth, and P. Gilch, The photoaddition of a psoralen to DNA proceeds via the triplet state, J. Am. Chem. Soc. 141, 13643 (2019).
- [83] J. Tatchen, M. Kleinschmidt, and C. M. Marian, Electronic excitation spectra and singlet– triplet coupling in psoralen and its sulfur and selenium analogs, J. Photochem. Photobiol. A 167, 201 (2004).
- [84] L. V. Slipchenko and A. I. Krylov, Singlet-triplet gaps in diradicals by the spin-flip approach: A benchmark study, J. Chem. Phys. 117, 4694 (2002).
- [85] M. Alessio and A. I. Krylov, Equation-of-motion coupled-cluster protocol for calculating magnetic properties: Theory and applications to single-molecule magnets, J. Chem. Theory Comput. 17, 4225 (2021).
- [86] N. Orms, D. R. Rehn, A. Dreuw, and A. I. Krylov, Characterizing bonding patterns in diradicals and triradicals by density-based wave function analysis: A uniform approach, J. Chem. Theory Comput. 14, 638 (2018).